Princeton Plasma Physics Laboratory

PPPL- 4376

PPPL- 4376

A Method to Simulate Linear Stability of Impulsively Accelerated Density Interfaces in Ideal-MHD and Gas Dynamics

Ravi Samtaney

February, 2009

Prepared for the U.S. Department of Energy under Contract DE-AC02-76CH03073.

Princeton Plasma Physics Laboratory
Report Disclaimers

Full Legal Disclaimer

This report was prepared as an account of work sponsored by an agency of the United States Government. Neither the United States Government nor any agency thereof, nor any of their employees, nor any of their contractors, subcontractors or their employees, makes any warranty, express or implied, or assumes any legal liability or responsibility for the accuracy, completeness, or any third party's use or the results of such use of any information, apparatus, product, or process disclosed, or represents that its use would not infringe privately owned rights. Reference herein to any specific commercial product, process, or service by trade name, trademark, manufacturer, or otherwise, does not necessarily constitute or imply its endorsement, recommendation, or favoring by the United States Government or any agency thereof or its contractors or subcontractors. The views and opinions of authors expressed herein do not necessarily state or reflect those of the United States Government or any agency thereof.

Trademark Disclaimer

Reference herein to any specific commercial product, process, or service by trade name, trademark, manufacturer, or otherwise, does not necessarily constitute or imply its endorsement, recommendation, or favoring by the United States Government or any agency thereof or its contractors or subcontractors.

PPPL Report Availability

Princeton Plasma Physics Laboratory:

http://www.pppl.gov/techreports.cfm

Office of Scientific and Technical Information (OSTI):

http://www.osti.gov/bridge

Related Links:

U.S. Department of Energy

Office of Scientific and Technical Information

Fusion Links

A method to simulate linear stability of impulsively accelerated density interfaces in ideal-MHD and gas dynamics

Ravi Samtaney

Princeton Plasma Physics Laboratory, Princeton University, P.O. Box 451, Princeton, NJ 08543-0451

Abstract

We present a numerical method to solve the linear stability of impulsively accelerated density interfaces in two dimensions such as those arising in the Richtmyer-Meshkov instability. The method uses an Eulerian approach, and is based on an unwind method to compute the temporally evolving base state and a flux vector splitting method for the perturbations. The method is applicable to either gas dynamics or magnetohydrodynamics. Numerical examples are presented for cases in which a hydrodynamic shock interacts with a single or double density interface, and a doubly shocked single density interface. Convergence tests show that the method is spatially second order accurate for smooth flows, and between first and second order accurate for flows with shocks.

Key words: Numerical linear stability, upwind method, Richtmyer-Meshkov
02.60.Cb, 04.30.Nk, 47.20.Cq, 52.57.Fg, 47.11.Df

1. Introduction

The Richtmyer-Meshkov (RM) instability is the subject of extensive experimental, theoretical and computational research because of its importance in technological applications such as inertial confinement fusion, as well as astrophysical phenomena such as supernovae collapse. A linear stability analysis was performed originally by Richtmyer [1], followed by experimental confirmation by Meshkov [2]. Richtmyer analyzed with the interaction of a shock wave with a perturbed contact discontinuity separating gases of different

densities and concluded that the perturbations on the contact discontinuity grew linearly with time. The linear analysis was further developed by Yang et al. [3] in which they also considered the case when the reflected wave is a rarefaction. Computing the linear response for both the reflected shock and reflected rarefaction cases requires special consideration for each case, and a different set of equations must be solved. Such simulations exploit the fact that the base state is a self-similarly evolving solution with a finite number of waves (a transmitted shock, a contact discontinuity, and either a reflected shock or a reflected rarefaction). The reflected and transmitted waves usually bound the computational domain for computing the linear quantities [3]. Analytical extensions of the linear stability analysis when the base state is more complicated than the one considered by Richmyer and Yang et al.have not been performed.

Hawley and Zabusky [4] provided a vortex dynamics interpretation to the RM instability. The density interface in gas dynamics is the site of baroclinically generated vorticity which is the essential driving mechanism of the instability. We will appeal to such an interpretation in discussing results from our numerical simulations. Recently, Samtaney [5] has shown that the RM instability is suppressed by the presence of a magnetic field, which was also confirmed analytically by Wheatley et al. [6]. The magneto-hydrodynamics (MHD) RM instability includes nonlinear MHD waves such as a slow-mode shock [5, 7]. Also, there have been the other gas dynamics configurations such as the Air-SF6 gas curtain experiments [8, 9]. Furthermore, there are situations where the density interface may not be sharp, i.e., there is a finite density gradient in moving from one fluid to another for which computing the linear stability may be desired. Extending the classical analytical way of linear stability in the context of MHD, the gas-curtain type configurations, or diffuse interface, is daunting. One way to compute these flows, at considerable computational expense, is to simulate the nonlinear equations in two dimensions with a small amplitude perturbation. An alternative possibility is to numerically compute the linear response by simulating the linearized equations. A generalized numerical approach for hyperbolic conservation laws was developed by Godlewski & Raviart [10] in which they formulate the approach in terms of finding measure solutions of the linearized equations, and proved, for a scalar conservation law, that the measure solution is recoverable as the limit of solutions of regularized linear systems in which the discontinuity of the basic solution has been smoothed out. Our approach is to simulate the system of linearized PDEs using an Eulerian approach with the regulariza-

tion that the the contact discontinuity and shocks are numerically smoothed out. The objective of this paper is precisely to develop an Eulerian numerical method to compute the linear stability of accelerated density interfaces which can be generally applicable to situations other than the classical one considered by Richtmyer. The outline of the paper is as follows. In Section 2 we present the equations of MHD in 2D, followed by the linearized system. It should be noted that the base state of the instability is time dependent and governed by a one dimensional nonlinear system of hyperbolic PDEs. In section 3, we present a numerical method to solve such a system. This is followed by numerical examples and convergence tests in Section 4, and a brief conclusion and recommendations for future work in Section 5.

2. Equations for the Base State and Perturbations

We begin by writing the equations of compressible MHD in conservative form in two dimensions as follows.

$$\frac{\partial U}{\partial t} + \frac{\partial F(U)}{\partial x} + \frac{\partial G(U)}{\partial y} = 0, \tag{1}$$

where the solution vector $U \equiv U(x, y, t)$ is,

$$U = \{\rho, \rho u, \rho v, \rho w, B_x, B_y, B_z, e\}^T, \tag{2}$$

where ρ is the density, $(\rho u, \rho v, \rho w)$ represents the momentum, (B_x, B_y, B_z) is the magnetic field, and e is the total energy per unit volume. The vectors $F(U)$ and $G(U)$ are the fluxes of mass, momentum, magnetic field and total energy in the x, and y directions, respectively, and are given by

$$F(U) = \begin{Bmatrix} \rho u \\ \rho u^2 + p_t - B_x^2 \\ \rho uv - B_x B_y \\ \rho uw - B_x B_z \\ 0 \\ uB_y - vB_x \\ uB_z - wB_z \\ (e + p_t)u - (\boldsymbol{B} \cdot \boldsymbol{u})B_x \end{Bmatrix}, \; G(U) = \begin{Bmatrix} \rho v \\ \rho uv - B_x B_y \\ \rho v^2 + p_t - B_y^2 \\ \rho vw - B_y B_z \\ vB_x - uB_y \\ 0 \\ vB_z - wB_y \\ (e + p_t)v - (\boldsymbol{B} \cdot \boldsymbol{u})B_y \end{Bmatrix}, \tag{3}$$

where p_t denotes the sum of the gas pressure and the magnetic pressure. The equations are closed by the following equation of state $e = \frac{p}{\gamma - 1} + \frac{\rho}{2} u_k u_k +$

$\frac{1}{2}B_kB_k$, The ratio of specific heats is denoted by γ and taken to be 5/3 through out this work.

Writing the solution as $U(x,y,t) = U^0(x,t) + \epsilon\ \hat{U}(x,t)\exp(iky)$, where $U^0(x,t)$ is a one-dimensional temporally evolving base state, and $\hat{U}(x,t)\exp(iky)$ is the perturbation. Substituting these back in to equation (1) we get the nonlinear system of hyperbolic PDEs in 1D governing the evolution of the base state.

$$\frac{\partial U^0}{\partial t} + \frac{\partial F(U^0)}{\partial x} \quad = \quad 0. \tag{4}$$

The perturbations are governed by the system of coupled linear wave equations written as

$$\frac{\partial \hat{U}}{\partial t} + \frac{\partial A(U^0)\hat{U}}{\partial x} \quad = \quad -ikS(U^0)\hat{U}, \tag{5}$$

where the wave speeds are given by the eigenvalues of $A(U^0)$, the Jacobian of the $F(U^0)$ with respect to U^0, and where $S(U^0)$ is the Jacobian of $G(U^0)$ with respect to U^0.

A consequence of Faraday's law is that an initially divergence free magnetic field leads to a divergence free magnetic field for all times corresponding to the lack of observations of magnetic monopoles in nature. This solenoidal property is expressed as $\nabla \cdot \mathbf{B} = 0$. The base state magnetic field is also required to be divergence free, and because this magnetic field is only a function of x, a direct consequence is that the x-component of the magnetic field B_x^0 is constant. The perturbed field has to satisfy

$$\frac{\partial \widehat{B_x}}{\partial x} + ik\widehat{B_y} = 0, \tag{6}$$

3. Numerical Method

We adopt the method of lines approach in which each equation is written as

$$\frac{\partial U}{\partial t} = R(U), \tag{7}$$

and employ either a second-order or a third-order TVD Runge-Kutta approach. The third-order TVD RK approach is outlined below (where n indicates the time step index):

$$U_0 \quad = \quad U^n$$

$$
\begin{aligned}
U_1 &= U_0 + \Delta t R(U_0) \\
U_2 &= \frac{3}{4}U_0 + \frac{1}{4}U_1 + \frac{\Delta t}{4}R(U_1) \\
U_3 &= \frac{1}{3}U_0 + \frac{2}{3}U_2 + \frac{2\Delta t}{3}R(U_2) \\
U^{n+1} &= U_3. \qquad (8)
\end{aligned}
$$

We use an upwind approach to solve the system given by equations (4) and (5). This upwind method presented below works in general for the MHD system for non-zero values of B^0; and for gas dynamics by setting $B^0 = 0$. We use a finite volume approach in which the one-dimensional domain $[x_l, x_r]$ is divided into finite volumes of size Δx each, indexed by i, and bound by faces at $i + \frac{1}{2}$ and $i - \frac{1}{2}$. The solution vectors U^0 and $\hat{U}$) are centered at the centroid of the finite volume. As discussed above, the divergence free condition implies that that one dimensional base state variable B_x^0 is constant. Thus, the number of equations for the base state actually decrease by one. We define another set of solution vectors $\bar{U}^0$ and $\tilde{U}$ which are defined as $\bar{U}^0$ and $\hat{U}$ but without the x-component of the magnetic field in each. The evolution of the x-component of the perturbed magnetic field, $\widehat{B_x}$, is treated separately.

We also define a flux vector $\bar{F}(U)$ which is the same as $F(U)$ but without the flux of the x-component of the base state which is zero. The flux derivative for the base state are numerically evaluated as:

$$
\left.\frac{\partial \bar{F}(U^0)}{\partial x}\right|_i = \frac{\bar{F}(U^0)_{i+\frac{1}{2}} - \bar{F}(U^0)_{i-\frac{1}{2}}}{\Delta x}, \qquad (9)
$$

where the flux $\bar{F}(U^0)_{i+\frac{1}{2}} \equiv \bar{F}(\bar{U}^0, B_x^0) \equiv \bar{F}(\bar{U}^0_{L,i+\frac{1}{2}}, \bar{U}^0_{R,i+\frac{1}{2}}, B_x^0)$, is obtained by

$$
\bar{F}(U^0)_{i+\frac{1}{2}} = \frac{1}{2}\left(\bar{F}(\bar{U}^0_{L,i+\frac{1}{2}}, B_x^0) + \bar{F}(\bar{U}^0_{R,i+\frac{1}{2}}, B_x^0)\right) - \frac{1}{2}\sum_{k=1}^{7}\alpha_k \boldsymbol{r}_k, \qquad (10)
$$

where $\alpha_k = \boldsymbol{l}_k \cdot (\bar{U}^0_{R,i+\frac{1}{2}} - \bar{U}^0_{L,i+\frac{1}{2}})$. $\boldsymbol{l}_k$ and $\boldsymbol{r}_k$ are left and right eigenvectors of matrix $\bar{A}$ which is the same as $A(U^0)$ excluding the row and column corresponding to B_x^0. $\bar{U}^0_{R,i+\frac{1}{2}}$ and $\bar{U}^0_{L,i+\frac{1}{2}}$ are left and right states obtained at the faces of the finite volumes by fitting linear profiles and van-Leer slope limiting.

The perturbed quantities, denoted as $\hat{U}$ above, are computed using the same method of lines approach. The right hand side for evolving $\tilde{U}$ consists of three terms:

$$\frac{\partial \tilde{U}}{\partial t} = R(\tilde{U}) = -\frac{\partial \bar{A}(U^0)\tilde{U}}{\partial x} - ik\bar{S}(U^0)\tilde{U} + C(U^0, \widehat{B_x}), \tag{11}$$

where $\bar{S}$ is S without the row/column corresponding to B_x^0, and C is a correction term described below. $\widehat{B}_x$ is evolved using

$$\frac{\partial \widehat{B_x}}{\partial t} = ik\left(\frac{(v^0 B_x^0 - u^0 B_y^0)}{\rho^0}\hat{\rho} + \frac{B_y^0}{\rho^0}\widehat{\rho u} - \frac{B_x^0}{\rho^0}\widehat{\rho v} + v^0\widehat{B_x} - u^0\widehat{B_y}\right). \tag{12}$$

We compute the flux $A(U^0)\hat{U}|_{i+\frac{1}{2}}$ by a seven-wave method for which we replace the matrix $A(U^0)$ with $\bar{A}$. The seven-waves correspond to the seven eigenvalues of $\bar{A}$ which are: $\{u^0, u^0 \pm c_f, u^0 \pm c_a, u^0 \pm c_s$ where the u^0 is the advection speed, and c_f, c_a, c_s correspond to the fast magneto-sonic, Alfvén, and slow magnetosonic speeds respectively. In our unified approach, when computing the gas dynamics cases (i.e., $B_x^0 = 0$), the fast and slow magnetosonic speeds smoothly reduce to the usual acoustic wave speed, and the Alfvén speed goes to zero. The flux term $\bar{A}\tilde{U}$ is computed using a flux-vector splitting approach, in which $\bar{A} = \bar{A}^+ + \bar{A}^-$, where $\bar{A}^+$ (resp. $\bar{A}^-$) is computing using the positive (resp. negative)eigenvalues of $\bar{A}$.

$$\left.\frac{\partial \bar{A}(U^0)\tilde{U}}{\partial x}\right|_i = \frac{\bar{A}(U^0)\tilde{U}|_{i+\frac{1}{2}} - \bar{A}(U^0)\tilde{U}|_{i-\frac{1}{2}}}{\Delta x}, \tag{13}$$

$$\begin{aligned}\bar{A}(U^0)\tilde{U}|_{i+\frac{1}{2}} &= \frac{1}{2}\left(\bar{A}_{i+\frac{1}{2}}\tilde{U}_{L,i+\frac{1}{2}}) + \bar{A}_{i+\frac{1}{2}}\tilde{U}_{R,i+\frac{1}{2}}\right) \\ &\quad -\frac{1}{2}|\bar{A}|_{i+\frac{1}{2}}(\tilde{U}_{R,i+\frac{1}{2}} - \tilde{U}_{L,i+\frac{1}{2}}),\end{aligned} \tag{14}$$

where $|\bar{A}| = \bar{A}^+ - \bar{A}^-$. Because, we have used the seven wave formulation, we still need to take into account the effect of $\hat{B}_x$ on the other variables. This is similar to the so-called "Stone correction" as it was suggested in the context of multi-dimensional MHD by Gardiner and Stone [11] and also used by Crockett et al. [12]. This correction term, denoted by $C(U^0, \widehat{B_x})$ in equation (11), is

$$C(U^0, \widehat{B_x}) = \{0, \gamma B_x^0, B_y^0, B_z^0, v^0, w^0, (\gamma B_x^0 u^0 + B_y^0 v^0 + B_z^0 w^0)\}^T \frac{\partial \widehat{B_x}}{\partial x}. \tag{15}$$

In particular, for $B_y^0 = B_z^0 = v^0 = w^0 = 0$, as used in the numerical examples later, the correction term is non-zero only for the x-momentum and the energy equations. These terms are evaluated using standard second-order central differences and added to the right hand side $R(\tilde{U})$ in the time stepping procedure. Finally, during each stage of the time integration procedure, the y-component of the perturbed magnetic field is replaced by

$$\widehat{B_y} = -ik\frac{\partial \widehat{B_x}}{\partial x}, \tag{16}$$

where the derivative on the right is evaluated using second-order central differences. This step ensures that the solenoidal property of the magnetic field is satisfied. If this step is omitted, the entire system of equations may be augmented by a non-conservative source term suggested by Falle et al. [13] and Powell et al. [14] for numerical stability. In our numerical examples discussed next, it made little difference if we enforced equation (16) or not. However, all results presented, the solenoidal constraint was strictly enforced.

4. Numerical Results

The main objective of the paper is to compute the linear response in the context of Richtmyer-Meshkov (RM) flows in which a hydrodynamic shock moves from a gas of one density into a gas of a different density. The interface between the gases may be a sharp one (i.e., the classical RM case) or one in which the density transition is done with a finite prescribed gradient. The interface needs to be perturbed with a single mode perturbation of wave number k. The numerical method described above also allows us to compute the linear stability of more than one density interface (as in the Air-SF6 gas curtain experiments), and also when the transmitted shock is allowed to reflect off an end wall and "reshock" the already shocked interface. Furthermore, the above numerical prescription also allows us to include a magnetic field and compute the linear stability of shocked density interfaces in MHD. For all cases considered in this section, the base state y- and z-components of the magnetic field and momentum are zero. The boundary conditions for the both the base state and the perturbed quantities are zero gradient in x for all cases except the re-shock case in which the normal component of the velocity is reflected at the right boundary.

4.1. Single Density Interface

In this section, we consider the interaction of a hydrodynamic shock with a single density interface for both the gas dynamic and MHD cases. For results shown in this section, the domain is $[x_l, x_r] = [-20 : 20]$, the shock is initialized at $x = -4$ and moves from left to right, and the density interface is centered at $x = 0$. The classical RM instability has a sharp interface which implies that the density changes in x as a Heaviside function. Consequently, the density perturbation $\hat{\rho}$ is a delta-function. In our Eulerian approach, we represent the Heaviside density function as:

$$\rho(x) = \frac{\rho_b + \rho_a}{2} + \frac{\rho_b - \rho_a}{\pi} \arctan\left(\frac{x}{\delta}\right), \tag{17}$$

where ρ_a (ρ_b) is the unshocked density to the left (right) of the interface, and δ is a measure of the smoothness applied to the sharp interface. The density perturbation is then given as:

$$\hat{\rho}(x) = \frac{\rho_b - \rho_a}{\pi\delta} \left(1 + \frac{x^2}{\delta^2}\right)^{-1}. \tag{18}$$

In the results discussed here, the Mach number of the incident shock is varied $M = 1.05, 1.25, 2.0$ which spans the shock strength from weak to moderate to strong shocks. The densities are chosen to be $\rho_a = 1$ and $\rho_b = 3$, i.e. an Atwood ratio of half. While we note that the Euler and ideal MHD equations are scale-free, in our computations, we fix the wave number of the perturbations as $k = 2\pi$ which imply a perturbation wavelength of unity. The interface smoothing parameter δ is chosen to be $0.05 - 0.1$. For the gas dynamic case, $B_x^0 = 0$ while for the MHD cases, the magnetic field is fixed such that the plasma beta $\beta = 2p/B_x^2 = 16$.

The base state in this example is such that the incident shock undergoes refraction at the density interface, resulting in a transmitted shock and a reflected shock. The subsequent evolution is self-similar in which all the waves (RS=reflected shock, TS=transmitted shock, CD=contact discontinuity) move with their own constant speed. The initial condition, and the base state after refraction is shown in Figure 1(a). As the incident shock traverses the interface, ideally it provides an impulse whereas in our smoothed interface we observe a large spike in the perturbed velocity. This spike is because of the finite interaction time between the incident shock and the density interface and is of no real physical consequence. In Figures 1(b) and 1(c), we plot the growth rate of the perturbed interface for the gas dynamic and the

MHD case. In these figures, $t = 0$ is the time when the incident shock has completely traversed the interface. The growth rate plots in the gas dynamics cases are predictable, with the usual fast initial growth followed by gradual decaying oscillations about an asymptotic value. The oscillations physically correspond to the reverberations of secondary waves which eventually decay. This behavior is consistent with the results of Richtmyer and Yang. The growth rate in the MHD cases are similar with those of gas dynamics but only in the very early stages. The growth rate quickly decays and oscillates about zero. The amplitude of the oscillations are larger for stronger incident shocks as expected. In Figure 1(d) the amplitude of the density interface for each shock strength are plotted and for comparison the saturation amplitudes predicted by the incompressible theory of Wheatley et al. [6] are shown as horizontal lines. Predictably, the numerical simulations agree well with the incompressible theory at low Mach numbers, with the differences growing with increasing Mach number.

4.1.1. Solution Details

In this section, we examine the spatial variation of the perturbed quantities for the $M = 1.25$ case for both the gas dynamic and MHD cases. For the gas dynamic case, in Figures 2(a), 2(b), we plot the x-component of the perturbed velocity, the y-component of the perturbed momentum at time $t = 18$. The density interface is centered at $x = 5$ where the peak $\hat{u}$ is observed. The signature of the vorticity is seen in the sharp gradient of $\widehat{\rho v}$ at the interface (denoted as 'VS' in Fig. 2(b)) which is the driving mechanism of the RM instability. There are oscillations behind the reflected and transmitted shocks which decay away as time progresses – a somewhat obvious behavior because hydrodynamic shocks are stable.

For the MHD case, we plot the x-component of the perturbed velocity, the y-component of the perturbed momentum, and the y- and x-components of the perturbed magnetic field at time $t = 18$ in Figures 2(c), 2(d), 2(e) and 2(f). The perturbed field $\widehat{B_y}$ shows evidence of Alfvén shocks which are also sites of the vortex sheets (denoted as 'VS' in Fig. 2(d)). This bifurcation of the vortex sheet in going from the gas to the MHD case was observed by Samtaney [5]. This bifurcation is due to the fact that for MHD jump conditions at contact discontinuities preclude shear whereas shocks in MHD support shear. Because the vorticity is transported away from the density interface, we expect that the interface, devoid of the driving mechanism, shows a decaying growth rate.

4.2. Reshocked Single Density Interface

A subject of recent interest has been the reshocking of the density interface by reflecting the transmitted shock from the right boundary [15]. Physically it may be of interest to predict the amplification of the linear growth rate after reshocking. For this case, the incident shock Mach number is $M = 1.25$ and the domain is $[x_l, x_r] = [-20 : 10]$ with reflecting boundary conditions at x_r. All other parameters are the same as in the previous sub-section. The growth rate is plotted in Figure 3. In this case, we plot the entire time history, not just after the incident shock has traversed the density interface. Hence, we see the short-lived spike in the growth rate which was discussed in the previous subsection, and which we believe to be of no physical consequence. It is interesting to note that in this case, after reshock, the shock moves from a region of higher density to one with a lower density. The reflected wave during the reshocking phase is now a rarefaction fan. The vorticity generated in during the reshocking phase is of opposite sign and the amplitude reverses phase. The growth rate changes sign after reshocking and saturates at a value about ten times larger than the first interaction.

4.3. Double Density Interface

In this section, we present results where instead of a single density interface we have two interfaces. The first density interface is located at $x = 0$ while the second one is located at $x = x_i = 4$. The density profile in x is given by:

$$\rho(x) = \rho_a + \frac{\rho_b - \rho_a}{\pi} \arctan\left(\frac{x}{\delta}\right) - \frac{\rho_b - \rho_a}{\pi} \arctan\left(\frac{x - x_i}{\delta}\right), \tag{19}$$

with the corresponding density perturbation given by

$$\hat{\rho}(x) = \frac{\rho_b - \rho_a}{\pi\delta}\left(1 + \frac{x^2}{\delta^2}\right)^{-1} \pm \frac{\rho_b - \rho_a}{\pi\delta}\left(1 + \frac{(x - x_i)^2}{\delta^2}\right)^{-1}, \tag{20}$$

where the $\pm$ indicates that the second density interface can be in-phase or out of phase with the first one. We show results for only the in-phase density interface. The base state at $t = 0$ and $t = 15$ is shown in Fig. 4(a). The growth rate for each density interface for the gas dynamic case is shown in Fig. 4(b). In this in-phase density perturbation the vorticity generated at the second interface is of opposite sign resulting in the phase reversal of the second interface. Before the transmitted shock exits the second interface, the

growth of the first interface proceeds as if the second interface did not exist due to the hyperbolic nature of the equations. Soon after the interaction with the second interface, a reflected rarefaction reaches the first one and amplifies the growth. Subsequently, there are internal reverberations inside the gas layer which modify the growth rate. In the MHD case, the first interaction is also as predicted with the growth rate decaying to zero, followed by an increase when the reflected rarefaction from the second interface reaches the first interface. Eventually the growth rate of both interfaces oscillates about zero.

4.4. Convergence Test

4.4.1. Smooth Density Interface

To verify that the solution converges with second order accuracy, we conduct a test of an impulsively started smooth density interface. The density profile is given by

$$\rho(x) = \frac{\rho_b + \rho_a}{2} + \frac{\rho_b - \rho_a}{2} \tanh\left(\frac{x}{\delta}\right), \tag{21}$$

and δ was chosen to be 0.5 and 1.0 for the gas dynamic and MHD cases, respectively. The impulse is provided at $t = 0$ by setting $u_0 = 0.5$ (corresponding to the impulse provided by a $M = 1.41$ shock). The base state in this case is simply a translating smooth density interface with no shocks. The domain of investigation is $[x_l, x_r] = [-20, 20]$ discretized with a grid of sizes: $3200, 1600, 800$, and 400. The solution corresponding to the 3200 mesh size is considered as an "exact" solution in this convergence analysis. Solutions at other resolutions are compared with this exact solution. Figure 5(a) shows the growth rate for the gas dynamic and the MHD case for mesh sizes of 3200 and 400. These are different initially because the interface is spread by different amounts in each case. The normalized amplitude of the interface is plotted for the MHD case in Fig. 5(b). The convergence plots show that the growth rate and amplitude are virtually indistinguishable for both the finest and the coarsest mesh considered here. The convergence analysis was done at time $t = 10$ by computing norms of the difference of the solution at the given resolution with the "exact" solution. The L_∞, L_1 and L_2 norms for each case are shown in Table 1 along with convergence rates in parenthesis. For this smooth case, the convergence rates exceed two for all the variables examined as we approach the finest mesh resolution.

Variable	Mesh	L_∞ (Rate)	L_1 (Rate)	L_2 (Rate)
$\hat{u}$	1600	1.64×10^{-3} (2.17)	2.42×10^{-3} (2.14)	2.42×10^{-4} (2.64)
	800	7.41×10^{-3} (1.25)	1.07×10^{-2} (1.29)	1.40×10^{-3} (1.73)
	400	1.77×10^{-2} (—)	2.61×10^{-2} (—)	4.63×10^{-3} (—)
$\widehat{B_x}$	1600	5.07×10^{-4} (2.20)	7.65×10^{-4} (2.31)	6.46×10^{-5} (2.74)
	800	2.32×10^{-3} (1.51)	3.80×10^{-3} (1.81)	4.33×10^{-4} (2.18)
	400	6.64×10^{-3} (—)	1.34×10^{-2} (—)	1.97×10^{-3} (—)
$\widehat{B_y}$	1600	5.78×10^{-4} (2.18)	8.19×10^{-4} (2.17)	7.35×10^{-5} (2.66)
	800	2.62×10^{-3} (1.31)	3.67×10^{-3} (1.43)	4.65×10^{-4} (1.85)
	400	6.49×10^{-3} (—)	9.92×10^{-3} (—)	1.67×10^{-3} (—)
$\hat{u}(G)$	1600	3.76×10^{-4} (2.34)	5.63×10^{-4} (2.35)	5.41×10^{-5} (2.85)
	800	1.90×10^{-3} (1.81)	2.87×10^{-3} (1.90)	3.89×10^{-4} (2.32)
	400	6.64×10^{-3} (—)	1.07×10^{-2} (—)	1.95×10^{-3} (—)
$\widehat{\rho v}(G)$	1600	2.04×10^{-3} (2.35)	3.05×10^{-3} (2.36)	2.87×10^{-4} (2.85)
	800	1.04×10^{-2} (1.84)	1.56×10^{-2} (1.92)	2.07×10^{-3} (2.36)
	400	3.74×10^{-2} (—)	5.93×10^{-2} (—)	1.06×10^{-2} (—)
$\hat{e}(G)$	1600	2.57×10^{-3} (2.35)	3.60×10^{-3} (2.36)	3.63×10^{-4} (2.85)
	800	1.30×10^{-2} (1.83)	1.85×10^{-2} (1.91)	2.61×10^{-3} (2.35)
	400	4.65×10^{-2} (—)	6.95×10^{-2} (—)	1.33×10^{-2} (—)

Table 1: Convergence test for the impulsively started smooth density interface. Variables suffixed with (G) are for the gas dynamic case while other variables are for the MHD case.

4.4.2. Shocked Single Density Interface

In this section, we present results from convergence tests for a $M = 1.25$ incident shock on a single density interface. The mesh sizes used in this study are: $6400, 3200, 1600$, and 800 points with the finest mesh solution considered as the "exact" solution. The growth rate at different mesh resolutions are plotted for both the MHD and gas dynamic cases in Figure 6. Except for the coarsest mesh considered here, the growth rates show very little difference. A convergence analysis was performed at time $t = 18$. The results of the convergence test are presented in Table 2. Due to the presence of discontinuities, it is not surprising that the convergence rate for the L_1 and L_2 norms are between first and second order.

5. Conclusion

In this paper, we presented an algorithm for solving the linear stability of shock-accelerated density interface such as those encountered in RM instability simulations. The approach is Eulerian, uses a somewhat traditional upwind approach and is relatively simple. Convergence studies indicate that the method is spatially second order accurate for smooth flows, and between first and second order accurate for flows with shocks. We presented examples from gas dynamics as well as MHD for a variety of scenarios: single and

Variable	Mesh	L_∞	L_1	L_2
$\hat{u}$	3200	0.0434 (1.22)	0.0198 (1.69)	0.00167 (2.05)
	1600	0.1009 (0.86)	0.0641 (1.28)	0.00693 (1.59)
	800	0.1833 (—)	0.1560 (—)	0.02082 (—)
$\widehat{B_x}$	3200	0.2161 (0.75)	0.0471 (1.34)	0.00645 (1.55)
	1600	0.3644 (0.56)	0.1194 (0.94)	0.01899 (1.07)
	800	0.5397 (—)	0.2296 (—)	0.03990 (—)
$\widehat{B_y}$	3200	0.03950 (0.74)	0.06121 (1.43)	0.00348 (1.61)
	1600	0.0658 (0.48)	0.1646 (0.86)	0.01061 (1.00)
	800	0.0914 (—)	0.2978 (—)	0.02123 (—)
$\hat{u}(G)$	3200	0.0448 (0.92)	0.0286 (1.68)	0.00245 (1.87)
	1600	0.0847 (0.86)	0.0914 (1.14)	0.00897 (1.43)
	800	0.1531 (—)	0.2016 (—)	0.02430 (—)

Table 2: Convergence test for a shocked density interface. The base state has shocks. Variables suffixed with (G) are for the gas dynamic case while other variables are for the MHD case. The convergence analysis was performed at $t = 18$.

double density interface, and reshocked single density interfaces. The gas dynamics growth rates are similar to those computed by earlier researchers. In the MHD case, the growth rate of the instability decays and oscillates with decreasing amplitude about zero. Furthermore, in MHD, the amplitude of perturbation saturates in agreement with previously published incompressible theory. The major appeal of the current approach is that it is quite simple to implement with no special consideration is required about the form of the solution of the underlying temporally evolving base state and is applicable to both gas dynamics and MHD. The present approach is easily extensible to flows with chemical reactions, with other time varying or constant accelerations of the interface (e.g. Rayleigh- Taylor instability) and for computing the linear stability of the interface in radially converging geometries (such as those encountered in inertial fusion).

Acknowledgments

This work was supported under the DOE SciDAC program (USDOE Contract no. DE-AC020-76-CH03073) performed at Princeton Plasma Physics Laboratory, Princeton University.

References

[1] R. D. Richtmyer. Taylor instability in shock acceleration of compressible fluids. *Comm. Pure and Appl. Math.*, XIII:297–319, 1960.

[2] Ye. Ye. Meshkov. Instability of a shock wave accelerated interface between two gases. *NASA Tech. Trans.*, NASA TT F-13074, 1970.

[3] Y. Yang, Q. Zhang, and D. H. Sharp. Small amplitude theory of Richtmyer-Meshkov instability. *Phys. Fluids*, 6(5):1856–1873, 1994.

[4] J. F. Hawley and N. J. Zabusky. Vortex paradigm for shock-accelerated density-stratified interfaces. *Phys. Rev. Lett.*, 63:1241–1244, 1989.

[5] R. Samtaney. Suppression of the Richtmyer-Meshkov instability in the presence of a magnetic field. *Phys. Fluids*, 15(8):L53–56, 2003.

[6] V. Wheatley, D. I. Pullin, and R. Samtaney. Stability of an impulsively accelerated density interface in magnetohydrodynamics. *Phys. Rev. Lett*, 95:125002, 2005.

[7] V. Wheatley, D. I. Pullin, and R. Samtaney. Regular shock refraction at an oblique planar density interface in magnetohydrodynamics. *J. Fluid Mech.*, 522:179–214, 2005.

[8] Jacobs J. W., Klein D. L., Jenkins D. G., and Benjamin R. F. Instability growth-patterns of a shock-accelerated thin fluid layer. *Phys. Rev.Lett.*, 70(5):583–586, 1993.

[9] Prestridge K., Rightley P. M., Vorobieff P., Benjamin R. F., and Kurnit N. A. Simultaneous density-field visualization and PIV of a shock-accelerated gas curtain. *Experiments in Fluids*, 29(4):339–346, 2000.

[10] E. Godlewski and P-A Raviart. The linearized stability of solutions of nonlinear hyperbolic systems of conservation laws A general numerical approach. *Mathematics and Computers in Simulation*, 50:77–95, 1999.

[11] T. A. Gardiner and J. M. Stone. An unsplit godunov method for ideal mhd via constrained transport. *J. Comput. Phys.*, 205:509–539, 2005.

[12] R. K. Crockett, P. Colella, R. T. Fisher, R. I. Klein, and C. F. McKee. An unsplit, cell-centered Godunov method for ideal MHD. *J. Comp. Phys.*, 203:422–448, 2005.

[13] S. A. E. G. Falle, S. S. Komissarov, and P. Joarder. A multidimensional upwind scheme for magnetohydrodynamics. *Mon. Not. R. Astron. Soc.*, 297(1):265–277, 1998.

[14] K.G. Powell, P.L. Roe, T.J. Linde, T.I. Gombosi, and D.L. DeZeeuw. A solution-adaptive upwind scheme for ideal magnetohydrodynamics. *J. Comp. Phys.*, 154:284–300, 1999.

[15] D. J. Hill, C. Pantano, and D. I. Pullin. Large-eddy simulation and multiscale modelling of a Richtmyer-Meshkov instability with reshock. *J. Fluid Mech.*, 557:29–61, 2006.

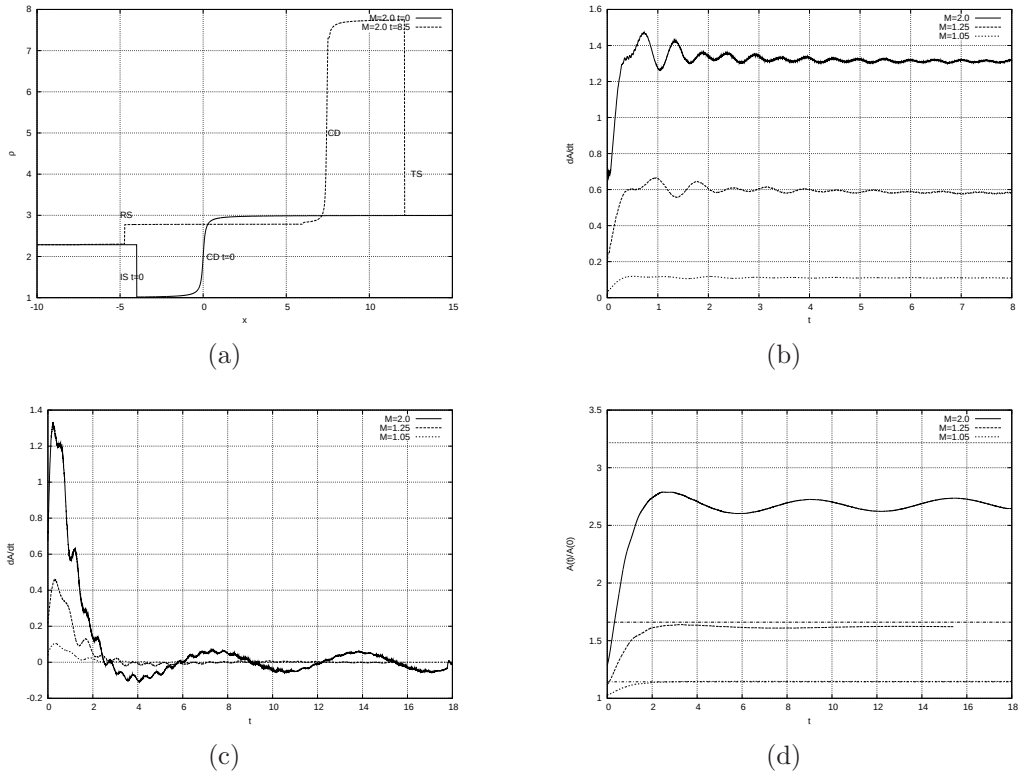

Figure 1: (a): Base state initial condition and after refraction. 'IS' is the incident shock; 'RS' and 'TS' are the reflected and transmitted shocks, respectively, after the interaction of 'IS' with the contact discontinuity 'CD'. (b) Growth rate for $M = 1.05, 1.25, 2.0$ shocks for the gas dynamic case. (c) Growth rate for $M = 1.05, 1.25, 2.0$ shocks for the MHD case. (d) Amplitude plots for the MHD case. The horizontal lines are the asymptotic amplitudes predicted by incompressible theory [6].

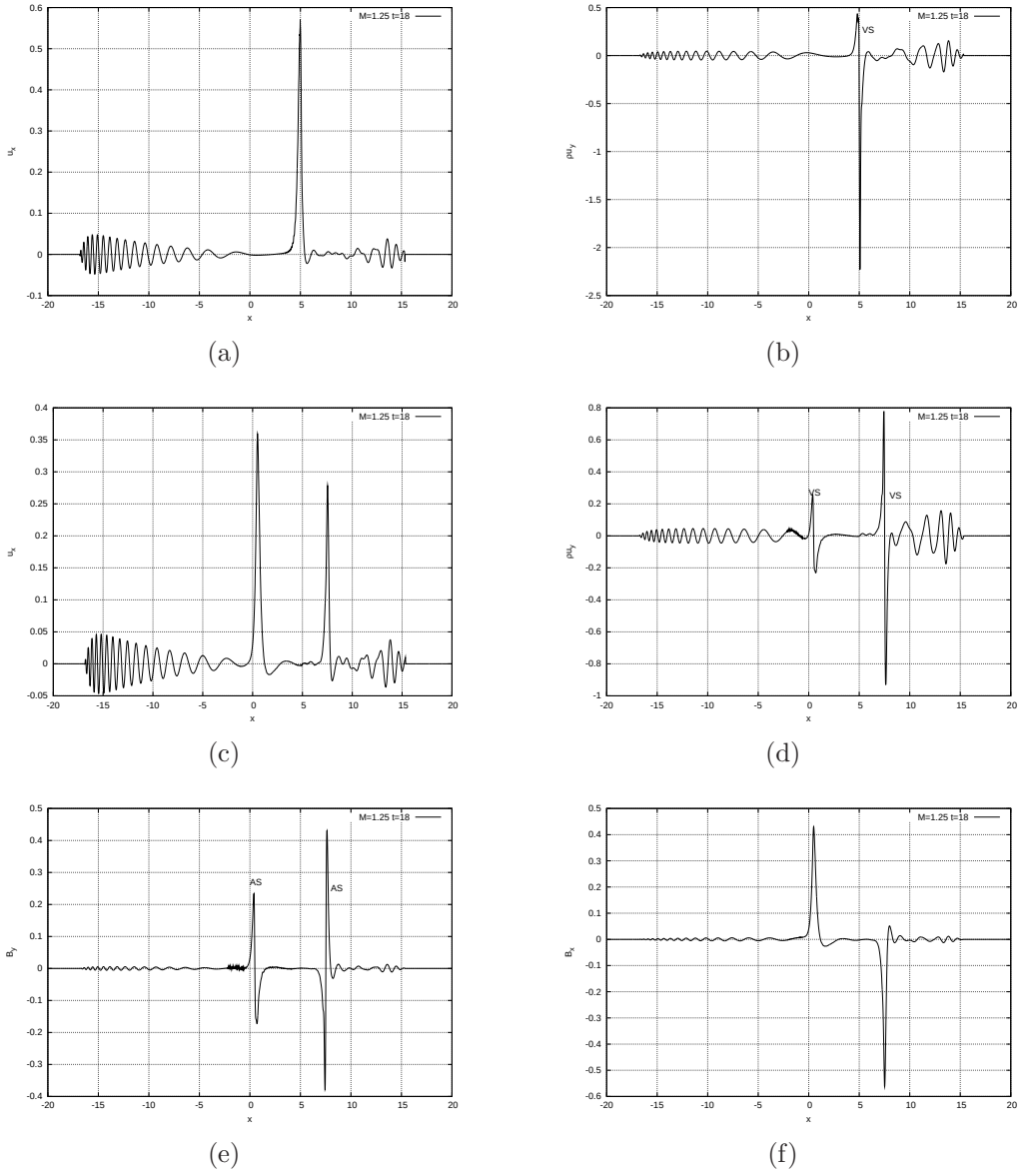

(a) (b) (c) (d) (e) (f)

Figure 2: (a): Perturbed x-component of the velocity for the gas case. (b) Perturbed y-component of the momentum for the gas case. 'VS' indicates the vortex sheet (c) Perturbed x-component of the velocity for the MHD case. (d) Perturbed y-component of the momentum for the MHD case. The vortex sheets are indicated by 'VS' coincident with the Alfv/'en shocks. (e) Perturbed y-component of the magnetic field. 'AS' indicate the Alfv/'en shocks. (f) Perturbed x-component of the magnetic field.

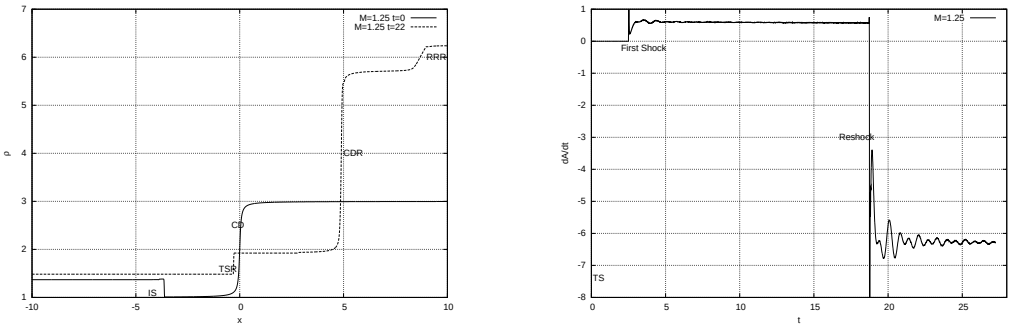

(a) (b)

Figure 3: (a) The base state shown at $t = 0$ and $t = 22.5$ (after reshocking the interface. 'IS' denotes the incident shock, 'CD' and 'CDR' denote the initial contact discontinuity and after reshock, 'RRR' is the reflected rarefaction after reshock, and 'TSR' is the transmitted shock after reshock. (b) The corresponding growth rate for this case.

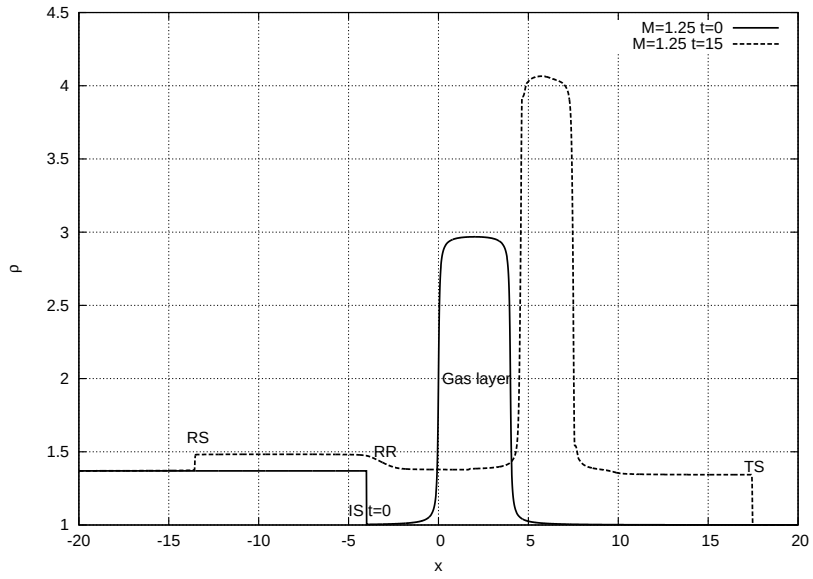

(a)

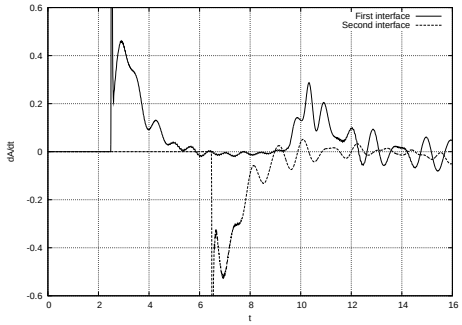

(b)

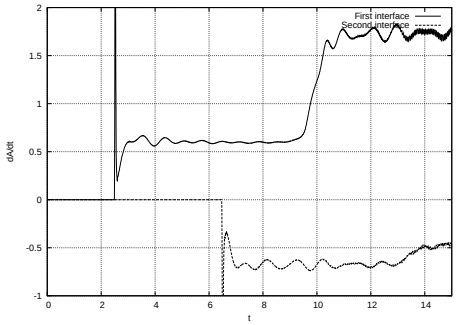

(c)

Figure 4: (a)Base solution shown at $t = 0$ and $t = 15$ for the density layer (two density interfaces) case. 'RS' is the reflected shock from the refraction at the first interface; 'RR' is the reflected rarefaction which emerges due to the refraction at the second interface; 'TS' is the transmitted which finally emerges from the density layer. (b) Growth rate for the MHD case. (c) Growth rate for the gas dynamic case.

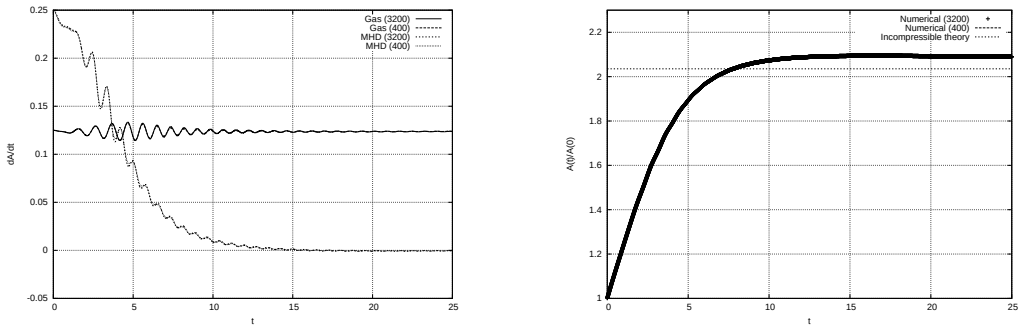

(a) (b)

Figure 5: (a)Growth rate for the impulsively started smooth density interface for the gas dynamic and MHD cases. For each case the finest mesh (3200) and coarsest mesh (400) solutions are plotted. (b) The normalized amplitude of perturbation for the MHD case. The incompressible theoretical result [6] is shown by the dotted horizontal line for reference. The coarsest and finest mesh solutions are virtually indistinguishable in these plots.

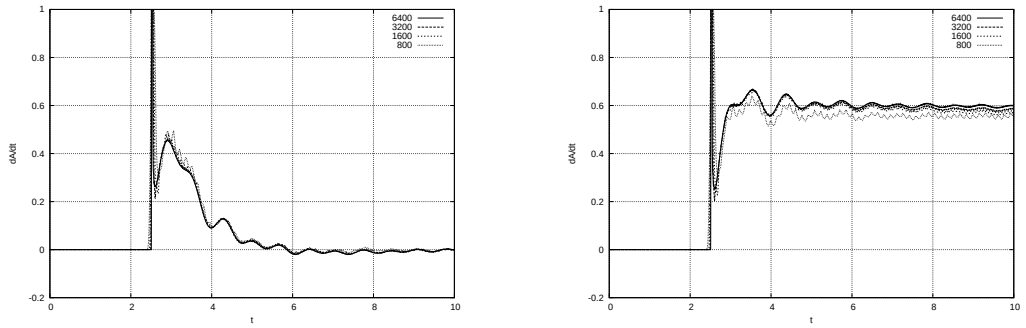

Figure 6: (a)Growth rate for the shocked single density interface for the MHD cases. (b)Growth rate for the shocked single density interface for the gas dynamic case. For each case the solutions at mesh resolutions of $6400, 3200, 1600$ and 800 are plotted.

The Princeton Plasma Physics Laboratory is operated
by Princeton University under contract
with the U.S. Department of Energy.

Information Services
Princeton Plasma Physics Laboratory
P.O. Box 451
Princeton, NJ 08543

Phone: 609-243-2750
Fax: 609-243-2751
e-mail: pppl_info@pppl.gov
Internet Address: http://www.pppl.gov